Available online at www.sciencedirect.com
SCIENCE DIRECT®
Proceedings of the Combustion Institute 30 (2005) 549–556
Proceedings of the Combustion Institute
www.elsevier.com/locate/proci

Large eddy simulation of a turbulent nonpremixed piloted methane jet flame (Sandia Flame D)

M.R.H. Sheikhi[a,*], T.G. Drozda[a], P. Givi[a], F.A. Jaberi[b], S.B. Pope[c]

[a] Department of Mechanical Engineering, University of Pittsburgh, Pittsburgh, PA 15261, USA
[b] Department of Mechanical Engineering, Michigan State University, East Lansing, MI 48824-1226, USA
[c] Sibley School of Mechanical and Aerospace Engineering, Cornell University, Ithaca, NY 14853-1301, USA

Abstract

Large eddy simulation (LES) is conducted of the Sandia Flame D [Proc. Combust. Inst. 27 (1998) 1087, Sandia National Laboratories (2004)], which is a turbulent piloted nonpremixed methane jet flame. The subgrid scale (SGS) closure is based on the scalar filtered mass density function (SFMDF) methodology [J. Fluid Mech. 401 (1999) 85]. The SFMDF is basically the mass weighted probability density function (PDF) of the SGS scalar quantities [Turbulent Flows (2000)]. For this flame (which exhibits little local extinction), a simple flamelet model is used to relate the instantaneous composition to the mixture fraction. The modelled SFMDF transport equation is solved by a hybrid finite-difference/Monte Carlo scheme. This is the first LES of a realistic turbulent flame using the transported PDF method as the SGS closure. The results via this method capture important features of the flame as observed experimentally.

Keywords: Large eddy simulation; Filter density function; Turbulent combustion; Nonpremixed flames

1. Introduction

There have been significant recent developments of subgrid scale (SGS) closures for large eddy simulation (LES) of turbulent reacting flows. Several recent reviews are available [4–12]. One such closure is via the filtered density function (FDF) methodology, first introduced by Pope [13]. This is the counterpart of the probability density function (PDF) method that has proven quite effective in Reynolds averaged simulations (RAS) [4,14]. This success is due to the inherent property of the PDF to provide complete statistical information about the variables. Due to this property, the FDF offers the ability to treat finite-rate chemistry and the turbulence-chemistry interactions. In comparison to RAS, the LES/FDF methodology provides a more detailed and reliable prediction of turbulent reacting flows and is better suited to account for the large scale unsteady phenomena, which are prevalent in combustion devices. The scalar FDF (SFDF) is considered by many investigators [15–19]. Its extension to account for variable density flows is via the scalar filtered mass density function (SFMDF) [3,20]. The velocity FDF (VFDF) is introduced by Gicquel et al. [21], and the velocity-scalar FDF (VSFDF) by Sheikhi et al. [22]. A recent review on the state-of-progress on LES/FDF is provided by Givi [12]. The outcome of these investigations has been encouraging,

* Corresponding author. Fax: +1 412 624 4846.
E-mail address: moh3@pitt.edu (M.R.H. Sheikhi).

1540-7489/$ - see front matter © 2004 The Combustion Institute. Published by Elsevier Inc. All rights reserved.
doi:10.1016/j.proci.2004.08.028

warranting further extension and application of this methodology in turbulent combustion.

In this work, we employ the FDF method for prediction of the piloted jet flame studied in the experiments of the Combustion Research Facility at the Sandia National Laboratories [1,23,24]. This flame has been the subject of broad investigations by other computational/modelling methodologies [2,25–28]. In the experiments, three turbulent flames are considered: Flames D, E, and F. The geometrical configuration in these flames is the same, but the jet inlet velocity is varied. In Flame D, the fuel jet velocity is the lowest, and the flame is close to equilibrium. The jet velocity increases from flames D to E to F, with noticeable non-equilibrium effects in the latter two. Flame D is considered in this work. The objective was to assess the predictive capability of the LES/FDF methodology in capturing the flow field and scalar mixing. This is a necessary step before consideration of the non-equilibrium flames (E and F).

2. Formulation

Sandia Flame D consists of a main jet with a mixture of 25% methane and 75% air by volume. The nozzle is placed in a coflow of air, and the flame is stabilized by a substantial pilot. The Reynolds number for the main jet is $Re = 22400$ based on the nozzle diameter $D = 7.2$ mm and the bulk jet velocity 49.6 m/s. All of the details regarding this flame are provided and regularly updated in the web site [2]. The methane–air reaction mechanism, as occurs in this flame, is taken into account via the "flamelet" model. This model considers a laminar, one-dimensional counterflow (opposed jet) flame configuration [8]. The detailed kinetics mechanism of the Gas Research Institute (GRI2.11) [29] is employed to describe combustion. At low strain rates, the flame is close to equilibrium. Thus, all of the thermo-chemical variables are determined by the "mixture fraction."

Formulation is based on the compressible form of the continuity, Navier-Stokes, energy (enthalpy) and mixture fraction conservation equations in a low Mach number flow [30]. These equations govern the space ($\mathbf{x} \equiv x_i$, $i = 1, 2, 3$) and time (t) variations of the fluid density $\rho(\mathbf{x}, t)$, the velocity vector $\mathbf{u} \equiv u_i(\mathbf{x}, t)$, the pressure $p(\mathbf{x}, t)$, the specific enthalpy $h(\mathbf{x}, t)$, and the mixture fraction $\xi(\mathbf{x}, t)$. We employ Fourier's law of heat conduction, Fick's law of diffusion, and we assume unity Lewis number. The molecular viscosity μ increases with temperature (T) to the power of 0.7. The magnitude of the molecular Schmidt (and Prandtl) number is $Sc = 0.75$.

For LES, we consider a spatially and temporally invariant positive filter $\mathcal{G}(\mathbf{x}' - \mathbf{x})$ of width $\Delta_{\mathcal{G}}$. The filtered value of the variable $Q(\mathbf{x}, t)$ is denoted by $\langle Q(\mathbf{x}, t)\rangle_\ell$, and its mass-weighted filtered value is denoted by $\langle Q(\mathbf{x}, t)\rangle_L = \langle \rho Q\rangle_\ell / \langle \rho\rangle_\ell$. The SFMDF of the mixture fraction is denoted by $\mathcal{F}_L(\psi, \mathbf{x}, t)$, where ψ denotes the (probability) composition domain of the mixture fraction. The SFMDF accounts for SGS statistics of only the scalar field. Thus, the closure of the SGS hydrodynamics must be provided by other means. Here, we employ a well-established gradient diffusion model, in which the SGS dynamic viscosity ν_t is modelled by the MKEV (modified kinetic energy viscosity) [3,31] model. In the transport equation governing the SFMDF, the effects of SGS convection are also modelled by an analogous gradient diffusion model. The SGS mixing is closed via the least mean square estimation (LMSE) model [32,33]. These are described in detail in our previous papers on SFDF [3,17]. The final, modelled SFMDF transport equation reads

$$\frac{\partial \mathcal{F}_L}{\partial t} + \frac{\partial [\langle u_i\rangle_L \mathcal{F}_L]}{\partial x_i} = \frac{\partial}{\partial x_i}\left[(\gamma + \gamma_t)\frac{\partial (\mathcal{F}_L/\langle \rho\rangle_\ell)}{\partial x_i}\right] + \frac{\partial}{\partial \psi}[\Omega_{\mathrm{m}}(\psi - \langle \xi\rangle_L)\mathcal{F}_L]. \quad (1)$$

Here, $\gamma = \mu/Sc$ is the molecular diffusivity, $\gamma_t = \frac{\langle \rho\rangle_\ell \nu_t}{Sc_t}$ is the SGS diffusivity, and $Sc_t = 0.75$ is the SGS Schmidt number. With the closure as such, the modelled scalar flux is consistent with those in most other (non-FDF) methods [34,35]

$$\langle \rho\rangle_\ell [\langle u_i \xi\rangle_L - \langle u_i\rangle_L \langle \xi\rangle_L] = -\gamma_t \frac{\partial \langle \xi\rangle_L}{\partial x_i}. \quad (2)$$

The term Ω_{m} is the SGS mixing frequency (as required in LMSE) and is modelled by [3,17] $\Omega_{\mathrm{m}} = C_\Omega(\gamma + \gamma_t)/(\langle \rho\rangle_\ell \Delta_{\mathcal{G}}^2)$, with $C_\Omega = 8$.

The relation between the thermo-chemical variables (denoted by the array $\boldsymbol{\phi}(\mathbf{x}, t)$) and the mixture fraction is provided by the flamelet library. In the context of the opposed jet flame, the library provides: $\boldsymbol{\phi} = \boldsymbol{\phi}(\xi, a)$ where a denotes the strain rate. For a fixed value of a, the SGS statistics of the thermo-chemical variables are determined from the SFMDF

$$\langle \boldsymbol{\phi}(\mathbf{x}, t)\rangle_L = \frac{1}{\langle \rho\rangle_\ell}\int \boldsymbol{\phi}(\xi)\mathcal{F}_L(\xi, \mathbf{x}, t)\,\mathrm{d}\xi. \quad (3)$$

A hybrid finite-difference (FD)/Monte Carlo (MC) scheme is employed to solve the coupled set of the SFMDF equation and the filtered hydrodynamic equations. In this scheme, the domain is discretized by FD grid points, and the SFMDF is represented via an ensemble of MC particles [36]. All of the hydrodynamic variables are determined on the FD points. A fourth order compact scheme is used for FD discretization of the compressible flow equations, as described in [37,38]. Transport of the MC particles and the change in their properties are described by a set

of stochastic differential equations (SDEs) similar to those describing a diffusion process [39]. The MC particles undergo motion in physical space by convection due to the filtered flow velocity and diffusion due to molecular and SGS diffusivities. The compositional value of each particle is changed due to SGS mixing. These are described by the SDEs:

$$\mathrm{d}x_i^+ = \left[\langle u_i\rangle_L + \frac{1}{\langle\rho\rangle_\ell}\frac{\partial(\gamma+\gamma_t)}{\partial x_i}\right]\mathrm{d}t + \sqrt{2(\gamma+\gamma_t)/\langle\rho\rangle_\ell}\,\mathrm{d}w_i, \tag{4}$$

$$\mathrm{d}\xi^+ = -\Omega_\mathrm{m}\left[\xi^+ - \langle\xi\rangle_L\right]\mathrm{d}t, \tag{5}$$

where x_i^+ and ξ^+ denote Lagrangian position and the composition (mixture fraction), respectively. The term w denotes the Wiener process [40]. The Fokker–Planck equation corresponding to Eqs. (4), (5) is equivalent to Eq. (1). Thus, the solution of these SDEs represents the FMDF in the probabilistic sense.

To understand the operational procedure, the elements of the computation are shown in Fig. 1. For simplicity, a two-dimensional domain is shown with fixed grid spacing of size of Δ. The MC particles are distributed randomly and are free to move within the domain as governed by Eq. (4). This transport is Lagrangian, thus the solution is free of constraints associated with typical simulation of convection on fixed grid points. Statistical information, e.g., filtered values, at any point is obtained by considering an ensemble of N_E computational particles residing within an ensemble domain of side length Δ_E centered around the points. For reliable statistics with minimal numerical dispersion, it is desired to minimize the size of ensemble domain and maximize the number of MC particles [14]. In this way, the ensemble statistics would tend to the desired filtered values. Transfer of information from the grid points to the MC particles is accomplished via interpolation. The transfer of information from the particles to the grid points is accomplished via ensemble averaging. In the hybrid scheme, some of the filtered quantities are obtained by MC, some by FD, and some by *both*. That is, there is a "redundancy" in determination of some of the quantities. This redundancy is very useful in monitoring the consistency of the simulated results [41]. In general, all of the equations for the filtered quantities can be solved by FD, where all of the unclosed terms are evaluated by MC. This process can be done at any filtered moment level [21]. Here, the filtered values of the mixture fraction and the temperature are used to establish consistency. Some results in this regard are presented in the next section. For more details we refer to [3,17,21,22]. In addition, the computational accuracy of the methodology is established by examining both the statistical and the dispersion errors [42]. In doing so, the correlation of the fluid density with distribution of the MC particles, the size of the ensemble domain, the number of particles within this domain, and the global distribution of the particles are monitored in a manner similar to those reported in our previous work [3,17,21,22].

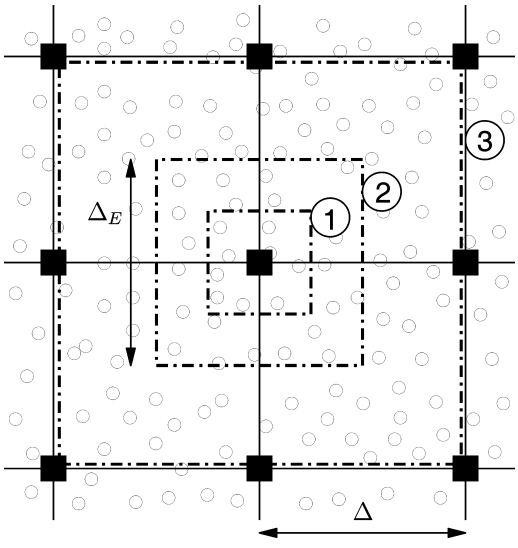

Fig. 1. Elements of computation as used in a typical LES/FDF. Solid squares denote the FD points, and the circles denote the MC particles. Also shown are three different ensemble domains.

3. Results

The flow variables at the inflow are set the same as those in the experiments, including the inlet profiles of the velocity and the mixture fraction. The flow is excited by superimposing oscillating axisymmetric and helical perturbations at the inflow. The procedure is similar to that of Danaila and Boersma [43], but the amplitude of forcing is set in such a way as to match the experimentally measured turbulent intensity of the streamwise velocity at the inlet. Simulations are conducted on a three-dimensional Cartesian mesh with uniform spacings in each of the three directions. Standard characteristic boundary conditions [44] are implemented in all of the FD simulations. The computational domain spans a region of $18D \times 10D \times 10D$ in streamwise (x), and the two lateral (y,z) directions, respectively. The number of grid points is $91 \times 101 \times 101$ in the x, y, and z directions, respectively. The filter size is set equal to $\Delta_\mathcal{G} = 2(\Delta x \Delta y \Delta z)^{(1/3)}$ where Δx, Δy, and Δz denote the grid spacings in the corresponding directions. The size of the ensemble

domain for evaluations of the filtered values from the MC solver is equal to the filter size. The particles are supplied in the inlet region and are free to move within the domain due to combined actions of convection and diffusion (molecular and SGS). There are approximately 48 MC particles at each grid point. As per results of extensive previous studies [3,17,21,22], this is sufficient to yield an excellent statistical accuracy with minimal dispersion errors. In total, there are about 3.4 million MC particles within the domain at all times. The simulation results are monitored to ensure that the particles fully encompass and extend well beyond regions of non-zero vorticity and reaction.

The flamelet table at a strain rate of $a = 100\,1/s$ is used to relate the thermo-chemical variables to the mixture fraction. This value is consistent with those used in previous PDF predictions of Sandia flames [45]. First, the consistency and accuracy of the computations are assessed. Next, the overall predictive capability of LES/SFMDF is demonstrated by comparing the flow statistics with the Sandia data. These statistics are obtained by long-time averaging of the filtered field during 6 flowthrough times. A total of 50,000 samples of each of the variables are collected in this recording period. The notations $\overline{Q}$ and RMS(Q) denote, respectively, the time-averaged mean and root mean square values of the variable Q. The simplest consistency check is via flow visualization. For example, Fig. 2 shows the instantaneous contours of the filtered mixture fraction field as obtained by the FD and the MC methods. The central jet lies in the middle along the axial coordinate, surrounded by a pilot where the temperature is the highest and encircled by the air coflow. The region close to inlet is dominated by the molecular diffusion, and the jet exhibits a laminar-like behavior. Farther downstream, the growth of perturbations is manifested by the formation of large-scale coherent vortices. The upstream feedback from the vortices created initially triggers further self-sustaining vortex rollup, and subsequent pairing and coalescence of neighboring vortices [46,47]. Due to the presence of helical instabilities, the instantaneous flow is asymmetric. The similarity of the results in the two figures is observed at all other times and is also observed for the temperature (not shown). This consistency is further assessed via establishing identical statistics of the redundant quantities as generated by the two methods. The capability of the method in predicting the hydrodynamics field is demonstrated by examining some of the (reported) flow statistics. The centerline mean and RMS values of the axial velocity are com-

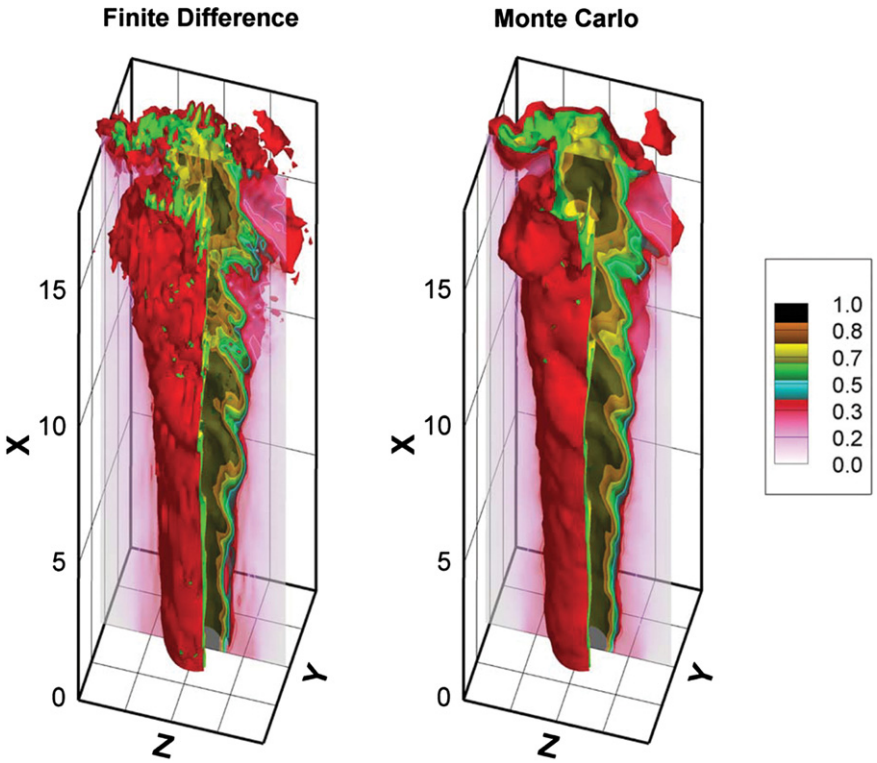

Fig. 2. Instantaneous contours of the filtered values of the mixture fraction as obtained by FD and MC simulations.

pared to experimental data in Fig. 3. This figure indicates that the flow is adequately excited, and the predicted results are in good agreement with data.

The statistics of the thermo-chemical variables are also compared with corresponding data. The measurements are exhaustive; here, only some sample results are shown. The radial ($r = \sqrt{z^2 + y^2}$) distribution of the mixture fraction is shown to compare well with data (Fig. 4A). Similar agreement is observed at other streamwise locations. The mean temperature values in Fig. 4B indicate over-prediction on the rich side. This is due to premixing of methane with air as also indicated previously [27]. The "resolved" RMS values of the mixture fraction and temperature are in good agreement with data. However, the "total" RMS values, including the contributions of both the resolved and the SGS fields, are higher than values reported experimentally. The contribution of the SGS to the total scalar energy is about 30%, which is expected in LES. The higher values of the total RMS values as predicted by LES/FDF are not due to MC numerical dispersion because the FD results do indeed yield the same values. The level of SGS variance can be decreased by increasing the magnitude of C_Q. However, this would not alter the total RMS values significantly. It is possible that some contribution of this variance is not included in the measurements due to finite probe size. Higher resolution measurements would determine the allocations of scalar variance to the resolved and SGS fields.

The statistics of the mass fractions (denoted by Y) of several of the species are compared with data in Fig. 5. Similar to the temperature results on the rich side, the reactants' mass fractions are under-predicted, while the products are over-predicted. The mean values of the mass fractions of the major and the minor species compare well with experimental data. All of the results indicate

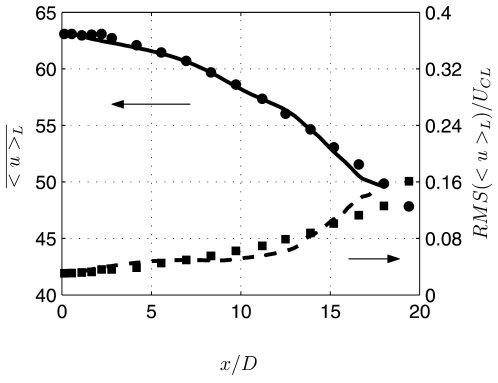

Fig. 3. The mean and RMS values of the axial velocity (m/s) at the centerline. U_{CL} denotes the mean axial velocity at the centerline, the symbols denote experimental data, and the lines denote the predictions.

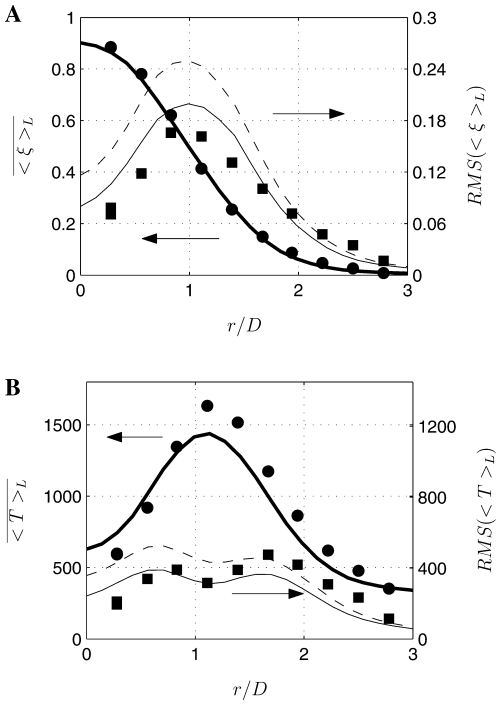

Fig. 4. Radial distributions of the mean and RMS values at $x/D = 15$. The symbols denote experimental data. The thick lines denote the mean values, the thin solid lines denote the resolved RMS values and the thin dashed lines denote total RMS values. (A) Mixture fraction, (B) temperature (K).

the adequacy of the flamelet table in relating the thermo-chemical variables to the mixture fraction, and also the good predictive capability of the SFMDF for this flame. The level of agreement of the RMS values of the mass fraction is the same as that presented in Fig. 4. Finally in Fig. 6 the PDFs of the resolved mixture fraction as predicted by LES are compared with those measured experimentally. It is encouraging to observe excellent agreements of both the peak and the range of the PDF. Similar agreements are observed at all the other locations.

The computational costs associated with LES/FDF depends, obviously, on the parameters of the simulations. For the case reported here, the simulations required about 110 h of CPU time on a SUN Fire 4800 with 6 processors. This includes the times required for consistency tests and ensemble averaging of data. The computational time for LES without including SGS effects [17] is about 10–12 times less. However, such simulations yield erroneous predictions and in many cases lead to numerical instabilities. For further comparative assessment of the computational requirements of the FDF in comparison to non-FDF methods, we refer to previous work [3,17,21,22].

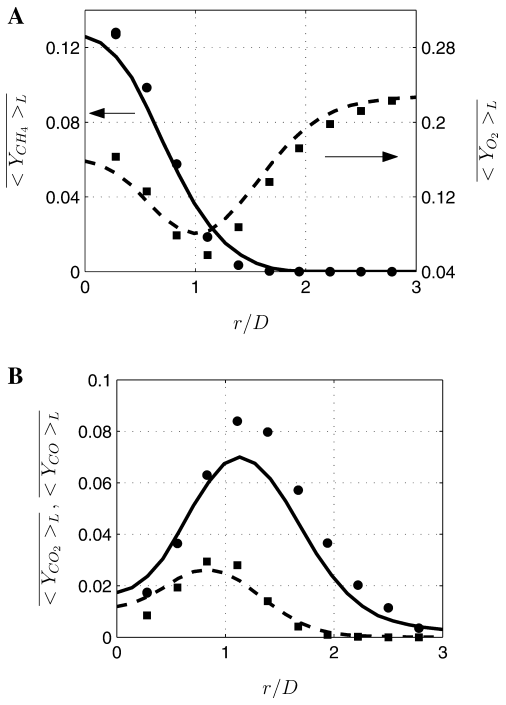

Fig. 5. Radial distribution of the mean values of the mass fractions at $x/D = 15$. The symbols denote experimental data. (A) Solid line, CH_4; dashed line, O_2; (B) solid line, CO_2; dashed line, CO.

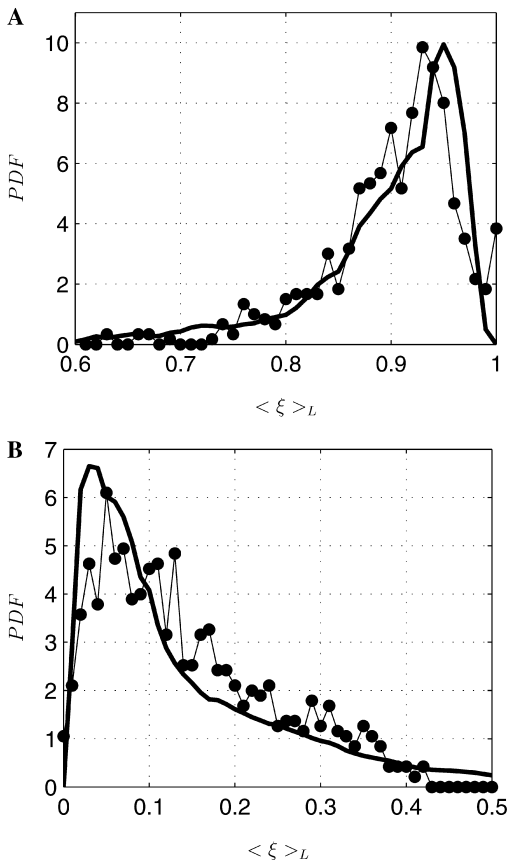

Fig. 6. PDF of filtered mixture fraction at $x/D = 15$ and different radial locations. The symbols and the thick lines denote experimental data and LES predictions, respectively. (A) $r/D = 0$, (B) $r/D = 1.67$.

4. Summary and concluding remarks

The filtered density function (FDF) methodology [12,13] is now at a stage that it can be used for prediction of complex turbulent reacting flows. This is demonstrated in this work by utilizing the simplest form of the FDF for large eddy simulation (LES) of a piloted, nonpremixed, turbulent, and methane jet flame (Sandia Flame D). For this near-equilibrium flame, the thermo-chemical variables are related to the mixture fraction. This is done by construction of a flamelet library (in a counter-flow jet flame) in which the chemical reaction is modelled by detailed kinetics [29]. It is useful to note that the approach here is fundamentally different from those followed in previous flamelet based SGS models. In most previous contributions [27,48–51], the FDF of the mixture fraction is *assumed* (e.g., β or other distributions). Here, a modelled transport equation for the mass weighted FDF of the mixture fraction [3] is considered. This equation is solved by a hybrid finite-difference/Monte Carlo method. After establishing the consistency and accuracy of the hybrid solver, the predictive capability of the overall scheme is assessed by comparison with experimental data. For these comparisons, the ensemble (long time averaged) values of the thermo-chemical variables are considered. It is shown that all of the mean quantities are, generally, predicted well. The resolved RMS of the variables also compare well with data. However, when the contribution of the subgrid scale (SGS) quantities is included, the experimental data are over-predicted.

There are two ways by which this work can be continued. First is extension of LES/SFMDF for prediction of flames that experience extinction (such as Sandia Flames E and F) and/or re-ignition. This would provide a more definitive assessment of the predictive capabilities of the FDF. Such simulations require consideration of finite-rate chemistry, as demonstrated in RAS/PDF simulations of Sandia flames [25,26]. Presently, it is not computationally feasible to implement detailed kinetics in such simulations. But implementation of reduced kinetics schemes using in situ adaptive tabulation, such as those used in RAS/PDF [25,26], is within reach. Second, it is desirable to implement the LES/VSFDF [22] for prediction of this (or other complex) flame(s). In VSFDF, the SGS convection appears in a closed form, thus the assumption of gradient

diffusion can be relaxed. This is also feasible within the near future. Accomplishments of both of these tasks can be expedited by further reduction of the computational requirements of the FDF. The present work establishes the capability of LES/FDF for accurate prediction of complex flames, warranting its further use for modelling of even more complex turbulent reacting flows.

Acknowledgments

This work is sponsored by the U.S. Air Force Office of Scientific Research under Grant F49620-03-1-0022 to the University of Pittsburgh and Grant F49620-00-1-0015 to Cornell University. Dr. Julian M Tishkoff is the Program Manager for both these grants. Acknowledgment is also made to the Donors of the Petroleum Research Funds administrated by the American Chemical Society for their support under Grant ACS-PRF 41222-AC9 to the University of Pittsburgh. Computational resources are provided by the Pittsburgh Supercomputing Center (PSC), and NCSA at the University of Illinois at Urbana.

References

[1] R.S. Barlow, J.I. Frank, Effects of turbulence on species mass fractions in methane/air jet flames, *Proc. Combust. Inst.* 27 (1998) 1087–1095.
[2] R.S. Barlow, Sandia National Laboratories, TNF Workshop website, 2004. Available from http://www.ca.sandia.gov/tnf/.
[3] F.A. Jaberi, P.J. Colucci, S. James, P. Givi, S.B. Pope, *J. Fluid Mech.* 401 (1999) 85–121.
[4] S.B. Pope, *Turbulent Flows*, Cambridge University Press, Cambridge, UK, 2000.
[5] A.W. Cook, J.J. Riley, in: M. Hafez, K. Oshima (Eds.), *Computational Fluid Dynamics Review 1998*, World Scientific, Singapore, 1998, pp. 914–931.
[6] R.W. Bilger, *Prog. Energy Combust. Sci.* 26 (4–6) (2000) 367–380.
[7] S. Menon, *Int. J. Engine Res.* 1 (2) (2000) 209–227.
[8] N. Peters, *Turbulent Combustion*, Cambridge University Press, Cambridge, UK, 2000.
[9] E.S. Oran, J.P. Boris, *Numerical Simulation of Reactive Flows*, second ed., Cambridge University Press, New York, NY, 2001.
[10] T. Poinsot, D. Veynante, *Theoretical and Numerical Combustion*, R.T. Edwards, Philadelphia, PA, 2001.
[11] D. Veynante, L. Vervisch, *Prog. Energ. Combust.* 28 (3) (2002) 193–301.
[12] P. Givi, *AIAA Paper* 2003-5081, 2003.
[13] S.B. Pope, *Proc. Combust. Inst.* 23 (1990) 591–612.
[14] S.B. Pope, *Prog. Energy Combust. Sci.* 11 (1985) 119–192.
[15] F. Gao, E.E. O'Brien, *Phys. Fluids A* 5 (6) (1993) 1282–1284.
[16] J. Réveillon, L. Vervisch, *AIAA J.* 36 (3) (1998) 336–341.
[17] P.J. Colucci, F.A. Jaberi, P. Givi, S.B. Pope, *Phys. Fluids* 10 (2) (1998) 499–515.
[18] X.Y. Zhou, J.C.F. Pereira, *Flow, Turbulence Combust.* 64 (2000) 279–300.
[19] C.M. Cha, P. Troullet, *Phys. Fluids* 15 (6) (2003) 1496–1504.
[20] S. James, F.A. Jaberi, *Combust. Flame* 123 (2000) 465–487.
[21] L.Y.M. Gicquel, P. Givi, F.A. Jaberi, S.B. Pope, *Phys. Fluids* 14 (3) (2002) 1196–1213.
[22] M.R.H. Sheikhi, T.G. Drozda, P. Givi, S.B. Pope, *Phys. Fluids* 15 (8) (2003) 2321–2337.
[23] P.A. Nooren, M. Versiuis, T.H. Van der Meer, R.S. Barlow, J.H. Frank, *Appl. Phys.* 71 (2000) 95–111.
[24] Sandia National Laboratories, Combustion Research Facility website, 2003, Available from http://www.ca.sandia.gov/crf/.
[25] Q. Tang, J. Xu, S.B. Pope, *Proc. Combust. Inst.* 28 (2000) 133–139.
[26] J. Xu, S.B. Pope, *Combust. Flame* 123 (2000) 281–307.
[27] H. Pitsch, H. Steiner, *Phys. Fluids* 12 (10) (2000) 2541–2554.
[28] H. Steiner, W.K. Bushe, *Phys. Fluids* 13 (3) (2001) 754–759.
[29] G.P. Smith, D.M. Golden, M. Frenklach, N.W. Moriarty, B. Eiteneer, M. Goldenberg, C.T. Bowman, R. Hanson, S. Song, W.C. Gardiner, V. Lissianski, Z. Qin, Available from http://www.me. berkeley.edu/gri_mech.
[30] F.A. Williams, *Combustion Theory*, second ed., The Benjamin/Cummings Publishing Company, Menlo Park, CA, 1985.
[31] J. Bardina, J.H. Ferziger, W.C. Reynolds, Department of Mechanical Engineering Report TF-19, Stanford University, Stanford, CA, 1983.
[32] E.E. O'Brien, in: P.A. Libby, F.A. Williams (Eds.), *Turbulent Reacting Flows, Chapter 5*, Springer-Verlag, Heidelberg, 1980, pp. 185–218.
[33] R. Borghi, *Prog. Energy Combust. Sci.* 14 (1988) 245–292.
[34] T.M. Eidson, *J. Fluid Mech.* 158 (1985) 245–268.
[35] P. Moin, W. Squires, W.H. Cabot, S. Lee, *Phys. Fluids A* 3 (1991) 2746–2757.
[36] S.B. Pope, *J. Comp. Phys.* 117 (1995) 332–349.
[37] J.P. Drummond, M.H. Carpenter, D.W. Riggins, in: S.N.B. Murthy, E.T. Curran (Eds.), *High Speed Propulsion Systems, vol. 137 of AIAA Progress Series*, American Institute of Aeronautics and Astronautics, 1991, Chapter 7, pp. 383–455.
[38] C.A. Kennedy, M.H. Carpenter, *Appl. Num. Math.* 14 (1994) 397–433.
[39] C.W. Gardiner, *Handbook of Stochastic Methods*, Springer-Verlag, New York, NY, 1990.
[40] S. Karlin, H.M. Taylor, *A Second Course in Stochastic Processes*, Academic Press, New York, NY, 1981.
[41] M. Muradoglu, S.B. Pope, D.A. Caughey, *J. Comp. Phys.* 172 (2001) 841–878.
[42] J. Xu, S.B. Pope, *J. Comp. Phys.* 152 (1999) 192–230.
[43] I. Danaila, B.J. Boersma, *Phys. Fluids* 12 (5) (2000) 1255–1257.
[44] T.J. Poinsot, S.K. Lele, *J. Comp. Phys.* 101 (1992) 104–129.
[45] K. Muradoglu, K. Liu, S. Pope, *Combust. Flame* 132 (2003) 115–137.

[46] P. Givi, J.J. Riley, in: M.Y. Hussaini, A. Kumar, R.G. Voigt (Eds.), *Major Research Topics in Combustion*, Springer-Verlag, New York, 1992, pp. 588–650.
[47] J.P. Drummond, P. Givi, in: J.D. Buckmaster, T.L. Jackson, A. Kumar (Eds.), *Combustion in High-Speed Flows*, Kluwer AcademicPublishers, The Netherlands, 1994, pp. 191–229.
[48] S.M. De Bruyn Kops, J.J. Riley, G. Kosály, A.W. Cook, *Combust. Flame* 60 (1998) 105–122.
[49] P.E. DesJardin, S.H. Franke, *Combust. Flame* 119 (1999) 121–132.
[50] A. Kempf, H. Forkel, J.Y. Chen, A. Sadiki, J. Janicka, *Proc. Combust. Inst.* 28 (2000) 35–40.
[51] F. Ladeinde, X. Cai, B. Sekar, B. Kiel, *AIAA Paper* 2001-0634, 2001.

Comments

J. P. Gore, Purdue University, USA. How are the particles leaving or entering the boundaries treated? Is the treatment consistent with physical laws at the boundary?

Reply. The MC particles leave the domain as they cross the boundaries. At the inlet, the particles enter the domain at a rate specified by fluid inflow rate.

•

Johannes Janicka, Technical University Darmstadt, Germany. (1) Could you comment on the applied simulation conditions? Of interest are the number of points, number of particles, and SGS-models for scalar and momentum. (2) Can you comment on the sharp of the SGS-pdf?

Reply. (1) The first part of the question is answered in the paper.

(2) The structure of the SGS-PDF depends on location/time. No "general" comments can be made about its shape.